# DETC2018-85712

# CONTROLLING ORIGAMI STABILITY PROFILE USING MAGNETS

Hongbin Fang\*, Tse-Shao Chang, K.W. Wang

Department of Mechanical Engineering University of Michigan Ann Arbor, MI 48109, USA

## **ABSTRACT**

Multi-stable structures and materials have attracted extensive research interests because they can provide a wide spectrum of adaptive properties and functionalities. Recently, origami has been identified as an important source for achieving multi-stability and has been exploited for developing unconventional mechanical metamaterials and metastructures. Once the crease pattern and the constituent materials have been specified for an origami structure, its multi-stability profile becomes unchangeable. On the other hand, a controllable profile would be desirable to endow the origami structures and origami metamaterials with further adaptability and versatility. This research investigates how to integrate magnets with origami to fundamentally alter the stability profiles. By embedding magnets into the origami facets or vertices, the magnetic potential energy would modify the original elastic potential energy landscape both quantitatively and qualitatively. Taking the stacked Miura-ori structures as examples, we show that different magnet assignments could either enrich the original bistable profile into a tri-stable or quad-stable profile, or simplify it into a mono-stable profile. Simultaneously, such magnet-induced evolutions of stability profile would trigger essential changes of the structure's mechanical properties, which are promising to be used for developing multi-functional devices or metamaterials/metastructures. In this paper, in addition to the analyses, proof-of-concept design and prototype are presented. The results of this research would open up a new path for designing origami structures and metamaterials with controllable stability profiles that can be harnessed for many novel applications.

## 1. INTRODUCTION

Origami, fundamentally a mechanism to fold 2-dimensional (2D) crease patterns to 3-dimensional (3D) shapes, has been widely adopted for designing and fabricating engineering systems such as biomedical devices [1–3], self-folding robots [4,5], large-scaled aerospace structures [6,7] and kinetic architectures [8]. Recently, origami also receives great success in developing mechanical metamaterials and metastructures with extraordinary properties and novel functionalities, which mainly originate from the folding-induced complex geometries and kinematics [9–12].

In particular, some origami structures possess multiple potential energy wells by elaborately prescribing the geometry patterns and precisely tuning the crease stiffness parameters. For example, in a stacked Miura-ori structure, double-well potential profile is achieved due to the non-unique correspondence between the folding angles of the two cells [13]; by connecting multiple units together, more potential minima can be obtained [14]. In generic degree-4 vertex origami sheets, the nonlinear relationships between folding angles also lead to complex energy landscapes with as many as five minima [15]. In these scenarios, rigid-foldability is ensured, where the facets are not deformed during folding but just rotate around the hinge-like creases. Multi-well potential landscapes can also be achieved in non-rigid-foldable origamis by incorporating the nonlinear geometry with the elastic facet deformations, with typical examples including the square-twist pattern [10], the Kresling pattern [16], and the origami balls [17]. Note that multi-well potential landscape is the defining characteristic of structural multi-stability. Therefore, origami offers a new solution to achieve bistability and multi-stability, which is completely different with the conventional mechanisms of multi-stability that are built upon either curved pre-buckled

<sup>\*</sup> Address all correspondence to this author: <a href="mailto:hongbinf@umich.edu">hongbinf@umich.edu</a>

beams or their close relatives such as pre-stressed bilayer shells and axially constrained springs [18–22].

The conventional buckled-beam mechanism simplicity in modeling, mechanical analysis, design and fabrication; however, due to the one-dimensional nature, they have limitations in constructing into truly 3D systems. The origami solution can therefore fill this gap by offering both sophisticated 3D geometries and rich multi-stability mechanisms. The multistable origami structures can stay at different configurations without external aids, making them appealing for shape morphing; they can exhibit different mechanical properties at different stable equilibria, letting them become adaptive to variable working environment; multi-stability can also trigger unconventional dynamics, leading to various dynamic applications including vibration control [23], energy harvesting [24,25], bandgap tuning [26], actuation [27,28], and sensing [29]. As a result, multi-stability has become an origami research interest, from bio-inspiration [30] to robotic application [17], from crease pattern design [15] to mechanical analysis [14], from statics [31] to dynamics [13], and from deployable structures [32] to metamaterial development [10,31].

Note that the multi-stability exhibits as an intrinsic property of an origami structure if the crease pattern and the constituent materials have been specified. In other words, for a given origami prototype, the underlying potential energy landscape cannot be quantitatively modified nor qualitatively changed. However, controlling the multi-stability profile (i.e., the multiwell potential landscape) without re-designing the crease pattern or re-fabricating the prototype is desirable in applications. For example, if the depths of the potential wells can be quantitatively changed, the critical force for switching among different stable states would become tunable to adapt to different environments and requirements. Furthermore, if the number and positions of potential wells can be altered, adaptive materials or structures with tailorable stable configurations can be developed for effective and efficient shape morphing. To achieve such controllability, additional active components or actuations are generally required. For example, a pressuredependent multi-stability characteristic was obtained in fluidic origami [33]. Upon pressurization, a Miura-ori stacked cell can switch its energy landscape between mono-stable and bistable; and stacking two pressurized cells could generate more than two stable configurations. While showing promising results, the pressure solution asks for a hermetic chamber inside the origami structure, which significantly limits its applications.

This research proposes using magnets to control the stability profile of origami structure. Note that some studies have already explored the multi-stability of systems with magnets, e.g., bistable magneto-active compliant mechanisms [34], cantilever beams coupled with magnets [35], etc. Magnets have also been combined with origami structures to achieve magnetic actuation and self-folding [36–39]. However, the effects of magnets on the structure's stability characteristics have not been concerned so far. By integrating magnets with origami structures, we find that the intrinsic potential energy

landscape originated from the elasticity of the constituent crease material will be quantitatively or even qualitatively changed by the additional magnetic potential energy. Hence, if the magnetic field strength and the magnetic polarization are tunable, for example, through the electromagnet approach, the overall energy landscape (i.e., the stability profile) of the integrated structure can be effectively controlled. Based on that, we can further tailor the mechanical properties accordingly. In addition to uncovering the fundamental mechanism, we show that such magnet-based approach possesses the advantage of design flexibility. For any origami structures, the sophisticated geometry could provide rich possibilities (e.g., on vertices or facet centers, etc.) to arrange multiple magnets, making this approach feasible in diverse origami-inspired structures and suitable for various applications like adaptive morphing and energy harvesting.

The rest of this paper will explore the magnet-coupled origami designs (Section 2), analyze the effects of different magnet configurations on the overall energy landscape through two examples (Section 3), and show a proof-of-concept design prototype (Section 4). Summary and discussions will be presented in Section 5.

### 2. MAGNET-COUPLED ORIGAMI DESIGNS

In this section, we introduce how to integrate magnets with origami structures. Note that a generic guideline for arranging magnets does not exit; here we provide a few examples to show the rich design possibilities.

An origami structures generally consists of a large number of vertices, creases, and facets that are available for arranging magnets. Taking a simple stacked Miura-ori (SMO) structure as an example, it consists of two Miura-ori cells, namely, bottom cell A and top cell B, characterized by crease length  $a_i$  and  $b_i$ , and a sector angle  $\gamma_i$ , where i takes 'A' or 'B' (Figure 1(a)). These parameters are not independent to each other but satisfy the following constraints for kinematic compatibility

$$b_{\rm A} = b_{\rm B} = b, \quad a_{\rm B} \cos \gamma_{\rm B} = a_{\rm A} \cos \gamma_{\rm A}.$$
 (1)

Folding of the structure is a one degree of freedom mechanism that can be described by the folding angles  $\theta_{\rm A}$  or  $\theta_{\rm B}$ , they relate to each other by

$$\theta_{\rm B} = \cos^{-1} \left( \cos \theta_{\rm A} \tan \gamma_{\rm A} / \tan \gamma_{\rm B} \right). \tag{2}$$

Hence, if taking  $\theta_{\rm A}$  as the independent variable, the outer dimensions of the SMO structure, i.e., the length L, the width W, and the height H, can be expressed as functions of  $\theta_{\rm A}$ :

$$L = \frac{2b\cos\theta_{A}\tan\gamma_{A}}{\sqrt{1+\cos^{2}\theta_{A}\tan^{2}\gamma_{A}}}, \quad W = 2a_{A}\sqrt{1-\sin^{2}\theta_{A}\sin^{2}\gamma_{A}},$$

$$H = a_{B}\sin\theta_{B}\sin\gamma_{B} - a_{A}\sin\theta_{A}\sin\gamma_{A}.$$
(3)

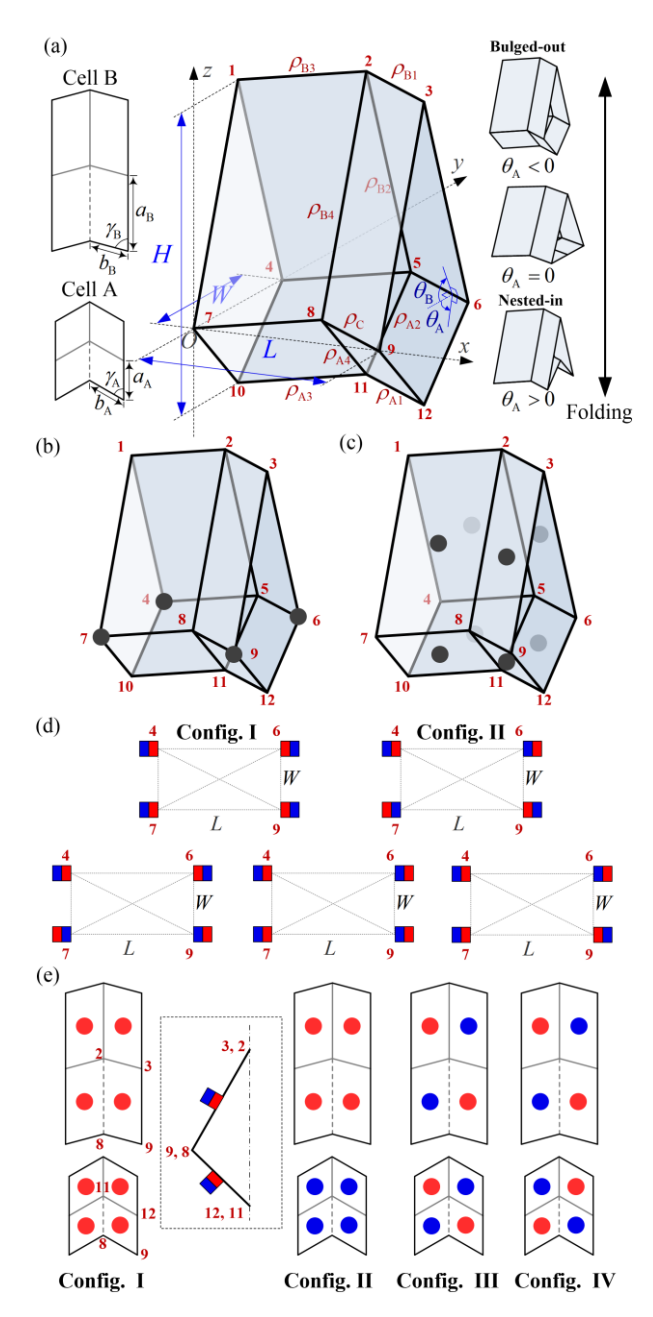


**FIGURE 1.** Geometry and designs of the magnet-coupled origami structures. (a) Geometry of a stacked Miura-ori structure, where all vertices are denoted by numbers from '1' to '12'; the external dimensions are denoted by L, W, and H; and the dihedral angles are denoted by  $\rho_{ki}$  (k=A,B; i=1,2,3,4). (b) Embedding magnets at four coplanar vertices '4', '6', '7', and '9'. (c) Embedding magnets at the facet centers. For simplicity, the magnetic poles are not denoted in (b) and (c). With different pole assignments, (d) and (e) show the possible magnet configurations based on the arrangements in (b) and (c), respectively. Note that in (e), the red and blue dots denote the poles that face inside the stacked structure (inset).

Overall, an SMO structure possesses 12 vertices, 20 creases, and 8 facets that can be utilized for arranging magnets. Figure 1(b) and (c) show two designs where the magnets are positioned at four coplanar vertices ('4', '6', '7', '9') and at the facet centers, respectively. With respect to folding, the relative distances among these vertices and facet centers would changes significantly, thus altering the magnetic energy of the system.

In addition to changing the magnet positions, the design can be further enriched by adjusting the magnetic polarization. For the first arrangement, theoretically, the four coplanar magnets can make up 16 different magnet configurations. However, considering the symmetry among the four magnets as well as the identity among certain pole-pole relationships, the 16 configurations can be deducted into 5 with unique pole assignments (Figure 1(d)). For the second arrangement, the eight magnets could constitute variegated 3D configurations; for illustration, we list a few examples in Figure 1(e).

It's worth pointing out that re-constructing the prototype is not needed to change the magnetic pole assignment. Instead, by employing electromagnets, the magnetic poles can be easily reversed by change the direction of electric currents. However, to uncover the mechanism, using permanent magnets is still acceptable in proof-of-concept analyses and experiments.

#### 3. THEORETICAL ANALYSIS

This section studies how magnets would change the intrinsic stability profile of origami structures. Specifically, this is achieved by examining the energy landscapes originated from the elastic potential and magnetic potential energies.

## 3.1. Elastic potential energy

With the rigid-folding assumption, the origami facets remain rigid during folding, and the creases are considered to be elastic hinges with prescribed torsional spring stiffness. For the SMO structure shown in Figure 1(a), we assign  $k_{\rm A}$  and  $k_{\rm B}$  as the torsional stiffness per unit length for the creases in cell A and cell B, respectively, and  $k_{\rm C}$  as the torsional stiffness per unit length at the connecting creases between the two cells. Then the torsional stiffness constants ( $K_{ki}$  and  $K_{\rm C}$ ) corresponding to each dihedral angle ( $\rho_{ki}$  and  $\rho_{\rm C}$ ) can be determined. Hence, the total elastic potential energy originating from the torsional creases is [13]

$$U_{E} = \frac{1}{2} \left[ \sum_{i=1}^{4} K_{Ai} \left( \rho_{Ai} - \rho_{Ai}^{0} \right)^{2} + \sum_{i=1}^{4} K_{Bi} \left( \rho_{Bi} - \rho_{Bi}^{0} \right)^{2} + 4K_{C} \left( \rho_{C} - \rho_{C}^{0} \right)^{2} \right].$$

$$(4)$$

In Eq. (4), the dihedral angles  $\rho_{ki}$  (k=A,B; i=1,2,3,4) and  $\rho_C$  can be expressed as functions of the folding angle  $\theta_A$ ;  $\rho_{Ai}^0$ ,  $\rho_{Bi}^0$  and  $\rho_C^0$  are the dihedral angles corresponding to the stress-free stable configuration at  $\theta_A = \theta_A^0$ , where no crease subjects to deformation. Specifically, we have

$$\rho_{\rm C} = \theta_{\rm B} - \theta_{\rm A}, \ \rho_{k1} = \rho_{k3} = \pi - 2\theta_{k},$$

$$\rho_{k2} = 2\arccos\frac{\sin\theta_{k}\cos\gamma_{k}}{\sqrt{1 - \sin^{2}\theta_{k}\sin^{2}\gamma_{k}}},$$

$$\rho_{k4} = 2\pi - \rho_{k2}, \ k = A, B.$$
(5)

For clarity, the configurations with  $\theta_A < 0$  and  $\theta_A > 0$  are denoted as bulged-out and nested-in, respectively (Figure 1(a)).

Note that by reasonably prescribing the crease stiffness and the stress-free folding angles, a double-well potential energy landscape can be obtained (e.g., Figure 2(c)), which signifies an elastic bistability profile. The origin of this bistability lies in the non-unique geometric relationship between the folding angles  $\theta_{\rm A}$  and  $\theta_{\rm B}$  showing in Eq. (2).

## 3.2. Magnetic potential energy

To analyze how the magnets contribute to the structure's overall potential energy landscape, a reliable magnetic field model is required. Amphère model and Gilbert model are always used to calculate the magnetic fields and the forces between magnets. Generally, the Amphère model is considered to be physically correct, in which the magnet is assumed to behave as if there is a macroscopic electric current flowing in loops in the magnet with the magnetic field normal to the loops. On the other hand, the Gilbert model is practically more convenient, which models the force between simple magnets as forces between magnetic poles, although the magnetic monopole does not exist.

Based on the Amphère model, if two magnets are small enough or sufficiently distant such that their shape and size are not important, then both magnets can be models as magnetic dipoles with magnetic dipole moments  $\mathbf{m}_1$  and  $\mathbf{m}_2$ . They can be treated as point dipoles in calculating their interaction potential energy H, which is given by

$$H_{\rm M} = -\frac{\mu_0}{4\pi |\mathbf{r}|^3} \left( 3(\mathbf{m}_1 \cdot \hat{\mathbf{r}})(\mathbf{m}_2 \cdot \hat{\mathbf{r}}) - \mathbf{m}_1 \cdot \mathbf{m}_2 \right), \tag{6}$$

where  $\mu_0$  is the permeability of free space,  $\mathbf{m}_1$  and  $\mathbf{m}_2$  are the vector dipole moments,  $\mathbf{r}$  is the vector between the two dipole centers,  $\hat{\mathbf{r}}$  is the unit vector parallel to  $\mathbf{r}$ , and  $|\mathbf{r}|$  is the distance between the two dipole centers.

In this research, as a preliminary modelling effort, the Gilbert model is employed instead to capture the qualitative interconnections between magnets. Specifically, cylindrical magnets are modeled into magnetic dipoles, with magnetic pole strength  $q=m/d=B_rA/\mu$ , where m is the magnetic dipole moment, d is the length of the magnets (i.e., the distance between the dipole), A is the cross-section area,  $B_r$  is the residual flux density, and  $\mu$  is the permeability of the medium (for air  $\mu=\mu_0=4\pi\times10^{-7}~{\rm T\cdot m/A}$ ). Note that here the magnetic dipole moment is due to two equal and opposite magnetic poles that are separated by a distance d, which is

similar to the electric dipole moment due to electrical charges. Such magnetic dipole moment is different with that in the Amphère model; it is physically incorrect, but is able to give a correct field of dipole. Based on this model, the force between two identical magnetic poles yields

$$F(x) = \frac{\mu q_m^2}{4\pi x^2},$$
 (7)

where x denotes the distance between two magnetic poles. Based on this, the magnetic potential energy between two identical poles can be obtained

$$U_{\rm M} = -\int F(x) dx = -\int \frac{\mu_0 q_m^2}{4\pi x^2} dx = \frac{\mu_0 q_m^2}{2\pi x}.$$
 (8)

where  $q_m$  takes positive if it is a north pole, and negative if it is a south pole.

Hence, if there are N identical magnets integrated with the origami structure, the system possesses 2N magnetic poles. By indexing the dipole of each magnet as (i, N+i), the total magnetic potential energy can be expressed as

$$U_{\text{M\_Total}} = \frac{1}{2} \left[ \sum_{\substack{i=1, i \neq j \\ i \neq N+j}}^{2N} \sum_{\substack{j=1 \\ j \neq N+i}}^{2N} \frac{\mu_0 q_m^2}{2\pi x_{ij}} \right]. \tag{9}$$

Then the total potential energy of the structure is

$$U = U_{\rm E} + U_{\rm M\ Total}.\tag{10}$$

In this study, the following magnet geometry parameters are used: radius R = 12.7 mm, length d = 6.35 mm. The residual flux density  $B_r$  is assumed to be tunable.

## 3.3. Example 1: Embedding magnets on coplanar vertices

In this example, four magnets are embedded with an SMO structure at the coplanar vertices '4', '6', '7', and '9', as shown in Figure 1(b) and 1(d). Specifically, the four magnets are aligned with lines '4-6' or '7-9', and one of the poles coincides with the vertex, while the other pole is d apart from the vertex (Figure 1(d)). Here, based on two magnet configurations, (I) and (II), four cases are studied. Each case shares the same origami geometry parameters (Table 1), but possess different stiffness parameters ( $k_A$ ,  $k_B$ , and  $k_C$ ) and magnetic residual flux density  $B_T$ .

Substituting Eq. (4) and (9) into Eq. (10), the total potential energy can be obtained in terms of the folding angle  $\theta_A$ . Based on the geometry relations given in Eq. (3), the total potential energy with respect to the outer dimensions L, W, and H can be expressed via the following parameterized equations

$$\begin{cases} L = L(\theta_A), & \begin{cases} W = W(\theta_A), & \begin{cases} H = H(\theta_A), \\ U = U(\theta_A); & U = U(\theta_A), \end{cases} \end{cases}$$

$$(11)$$

Moreover, the corresponding force-displacement relations in the L, W, and H directions can be obtained via

FIGURE 2. The potential energy profiles and the corresponding force-displacement relationships of the magnetcoupled origami structures (Example 1). The magnets are embedded at the four coplanar vertices (see Figure 1(b) and 1(d)). (a), (b) Case 1, with magnet configuration I, where the force-length relationship experience a qualitative change due to the embedded magnets. (c), (d) Case 2, with magnet configuration I, where the elastic bistability is changed to a mono-stable profile by the magnets. (e), (f), Cases 3 and 4, with magnet configuration II, where the elastic bistability can be changed to a quad-stable profile or another bistable profile by magnets of different pole strengths. In these figures, the direction of force is indicated in the inset, and the potential wells (aka stable states) are denoted by empty circles.

Height H (mm)

With Eq. (11) and Eq. (12), we are able to examine the potential energy landscapes and the force-displacement relationship in specific directions.

For Case 1 (with magnet configuration I), the potential energy and the force-displacement relationship are examined in the length (L) direction. Note that with the embedded magnets at the vertices, the total potential energy is upraised, especially at the regions with small length. Hence, when compressing the

**TABLE 1**. Origami and magnets parameters (Example 1)

	Par.	Values	Par.	Values
Origami geometry	$a_{\rm A} = b_{\rm A} = b_{\rm B}$	25.4 mm	$\gamma_{ m A}$	60°
	$a_{\mathrm{B}}$	31.75 mm	$ heta_{\!\scriptscriptstyle A}^{0}$	57°
Case 1 (Config. I)	$k_{\rm A} = k_{\rm C}$	0.5 N	$k_{\mathrm{B}}$	0.5 N
	$B_r$	1.48 T		
Case 2 (Config. I)	$k_{\rm A} = k_{\rm C}$	0.001 N	$k_{\mathrm{B}}$	0.05 N
	$B_r$	1.48 T		
Case 3 (Config. II)	$k_{\mathrm{A}} = k_{\mathrm{C}}$	0.035 N	$k_{\scriptscriptstyle  m B}$	1.75 N
	$B_r$	1.48 T		
Case 4 (Config. II)	$k_{\mathrm{A}} = k_{\mathrm{C}}$	0.035 N	$k_{\mathrm{B}}$	1.75 N
	$B_r$	2.96 T		

reaction force will increase to an extremely large value. This is qualitatively different with the structure without magnets.

For Case 2 (with the magnet configuration I but different crease stiffness), before embedding the magnets, the SMO structure possess elastic bistability in the height direction. By integrating the magnets, the double-well potential energy landscape is changed to a mono-well landscape, signifying a transformation of the stability from bistable to mono-stable. accordingly. the force-height curve Hence. changes qualitatively. For the structure without magnets, there are two stable states and a segment with negative stiffness; while for the structure with magnets, the number of stable states reduces to one.

For Case 3, magnet configuration II is used. Without the magnets, the SMO structure also shows elastic bistability. By adding the magnets with pole strength  $q_m$  ( $B_r = 1.48 \, \mathrm{T}$ ), surprisingly, the structure exhibits a quad-stable profile. In addition to the original two stable wells, the structure receives another two potential energy minima when the structure is folded toward flat (i.e.,  $\theta_A \to \pm 90^\circ$ ). This is induced by the strong magnetic attraction as  $L \to 0$  when  $\theta_A \to \pm 90^\circ$ .

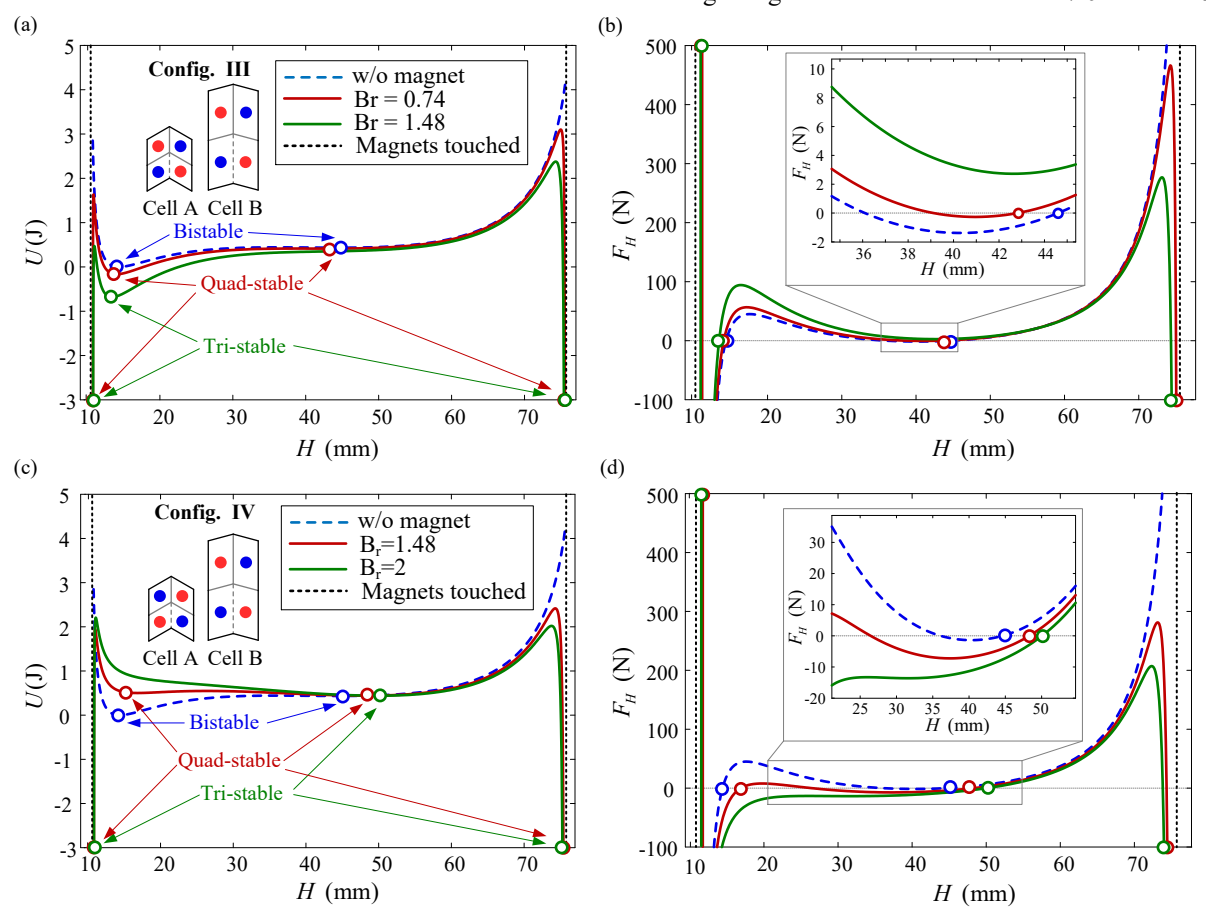


**FIGURE 3**. The potential energy profiles and the corresponding force-displacement relationships of the magnet-coupled origami structures (Example 2). The magnets are embedded at the eight facet centers (see Figure 1(c) and 1(e)). (a), (b) Case 1, with magnet configuration III; (c), (d) Case 2, with magnet configuration IV. In these two cases, the elastic bistability can be changed to a quad-stable profile or a tri-stable profile by magnets of different pole strengths. In these figures, and the potential wells (aka stable states) are denoted by empty circles.

At these two states, extremely large forces are needed to separate the stuck magnets.

For Case 4, with the same origami parameters and magnet configuration as Case 3, the structure loses the original two potential wells when the magnetic pole strength is doubled to  $2q_m$  (i.e.,  $B_r = 2.96 \, \mathrm{T}$ ). In such scenario, the structure becomes bistable again, where the two stable states locate at the positions with minimum and maximum height when  $\theta_4 \rightarrow \pm 90^\circ$ .

The above four cases well demonstrates how magnets could be exploited for controlling the origami structure's stability profile. On one hand, even the stability profile is not qualitatively changed, the corresponding force-displacement relationship could experience significant changes due to the additional attracting/repelling magnetic forces (Case 1). On the other hand, the magnetic potential energy could fundamentally change the total energy landscape by erasing the two elastic potential wells (i.e., change the elastic bistability to monostability, see Case 2), or by adding additional potential energy minima (i.e., change the elastic bistability to multi-stability, see Case 3), or a combination (Case 4).

# 3.4. Example 2: Embedding magnets on facet centers

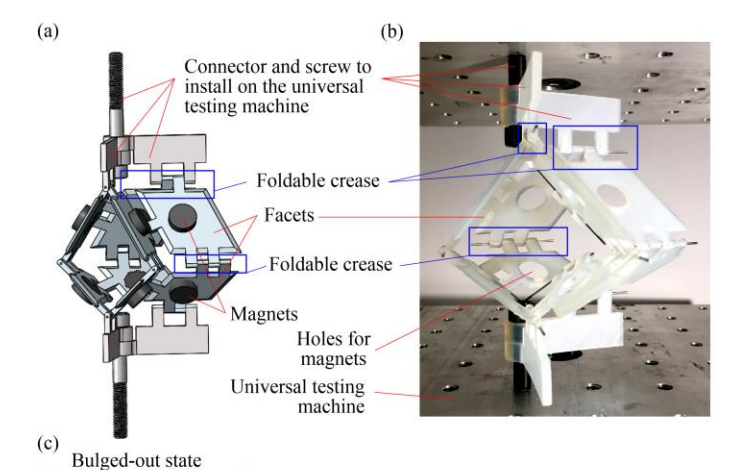
In this example, the magnets are embedded at the eight facet centers. As demonstrated in Figure 1(c) and 1(e), each magnet is perpendicular to the facet, with one of its side fitting with the facet (see inset of Figure 1(e)). Note that even with identical magnets, the possible configurations are various and abundant. Here, through two case studies (with detailed parameters listed in Table 2), we show again that different magnet configurations (including different pole strengths and different magnetic polarization) could induce different stability profiles.

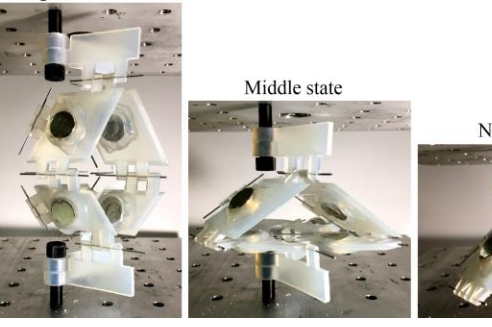
With Eq. (11) and (12), the potential energy landscape in the height (H) direction and the corresponding force-height relationship can be obtained and are plotted in Figure 3.

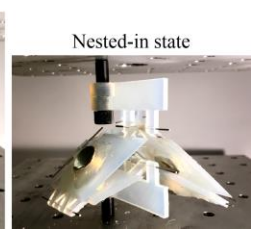
For Case 1 (with magnet configuration III), when the magnets are not embedded, the SMO structure shows elastic bistability. By adding the magnets with pole strength  $q_{m}$  $(B_r = 0.74 \text{ T})$ , the original two stable wells are remained, and the structure gains two new potential energy minima when the structure is folded toward the maximum and minimum height. Hence, the magnet-coupled SMO structure becomes quadstable. It is worth pointing out that practically the size of the magnets cannot be ignored, because the magnets may touch each other before the origami structure reaches the maximum or minimum height (i.e.,  $\theta_A \rightarrow \pm 90^\circ$ ). Hence, folding has to be stopped at the touching points, denoted by the dotted vertical lines in Figure 3. The new potential energy minima are generated by the strong magnetic attracting forces since the distance between the magnets are close. If the magnetic pole strength is doubled (with  $B_r$  rising from 0.74 T to 1.48 T), one of the elastic potential well vanishes, giving rise to a tristable profile.

TABLE 2. Origami and magnets parameters (Example 2)

	Par.	Values	Par.	Values
Origami geometry	$a_{\rm A} = b_{\rm A} = b_{\rm B}$	38.1 mm	$\gamma_{ m A}$	60°
	$a_{\scriptscriptstyle  m B}$	47.62 mm	$ heta_{\!\scriptscriptstyle A}^{^{\;0}}$	40°
	$k_{\mathrm{A}} = k_{\mathrm{C}}$	1 N	$k_{\scriptscriptstyle  m B}$	20 N
Case 1 (Config. III)	$B_r$	0.74 T, 1.48 T		
Case 2 (Config. IV)	$B_r$	1.48 T, 2 T		







**FIGURE 4.** Proof-of-concept design and prototype of the magnet-coupled SMO structure. (a) SolidWorks design of the prototype and the connector; (b) the 3D-printed prototype without magnets; (c) the 3D-printed prototype with magnets, showing in a bulged-out state, a middle state, and a nested-in state.

For Case 2 (with magnet configuration IV), similar phenomena as Case 1 are observed, where the elastic bistability can be changed to tri-stable or quad-stable profiles. However, due to the different magnet polarization, the lost elastic potential well is different.

Overall, the above two examples well demonstrate how magnets can be incorporated into origami structures to control the stability profiles. Such capability is appearing in origami application. Particularly, considering that changing magnet pole directions and pole strengths can be easily achieved via electromagnetics, the feasibility of the proposed approach can be well ensured.

## 4. PROOF-OF-CONCEPT PROTOTYPES

In this section we show a design and prototype of the magnet-coupled SMO structure to prove the concept. The second example is specifically designed and prototyped. Figure 4(a) shows the overall SolidWorks design of the magnet-coupled SMO structure. Holes are reserved at the facet centers for embedding magnets. The foldable creases are realized through fine pins that connect each two facets, so that the facets can freely rotate with respect to the pins. To experimentally show the stability changes due to magnets, tension and compression tests are needed on universal testing machine. To that end, additional connectors are designed.

The proof-of-concept prototype is fabricated through 3D-printing technique and human assemble. With the Form 2 printer, Durable Photopolymer Resin is used to print the origami facets (with facet thickness 2.54 mm, sector angle  $\alpha_A=60^\circ$ , and crease lengths  $a_A=b_A=b_B=38.1\,\mathrm{mm}$ ,  $a_b=1.5a_A$ ). Figure 4(b) firstly shows the SMO prototype without the magnets. By embedding permanent magnets, Figure 4(c) displays the magnet-coupled prototype, showing in three states: a bulged-out state, a middle state, and a nested-in state.

### 5. SUMMARY AND DISCUSSION

This research reports a new method to control origami structure's stability profiles by utilizing magnets. We show that by embedding magnets into origami structures, the intrinsic elastic potential energy landscape can be significantly changed. In addition to quantitatively raising or lowering the total energy landscape, the magnetic potential energy could qualitatively change the overall energy landscape by removing the original elastic potential wells or adding additional potential minima. Such changes of energy landscapes suggest the fundamental alteration of the origami structure's stability profile. Through two examples, one with magnets embedded at the four coplanar vertices of a SMO structure, and the other with magnets embedded at the eight facet centers, the capability of controlling stability profiles via magnets is demonstrated. Rich stability transitions are observed, including degeneration from bistability to mono-stability, and various changes from bistability to tristability and quad-stability. Proof-of-concept design and prototype is also proposed in this paper to illustrate the feasibility.

Previous studies have demonstrated that origami is a good platform to design structures and metamaterials with extraordinary stability profiles originating from folding geometries. Such discoveries provide a new way to design multi-stable metastructures and metamaterials that no longer rely on structural instabilities (e.g., pre-buckled beam and pre-stressed shells). However, the obtained stability profiles are intrinsic properties of the origami structures; once the crease patterns and the elastic crease materials have been prescribed,

they become unchangeable. They cannot adapt to variable working environments, nor endow the structures with multiple functionalities. The proposed controlling method therefore fundamentally advances the state of the art. Without redesigning or re-fabricating the structures, the potential energy landscapes can be effectively controlled via magnets. By adjusting the magnet configuration (i.e., changing the magnetic field strengths and magnetic polarization), the energy landscapes can be qualitatively and quantitatively controlled. Such control can be easily implemented by tailoring the electric currents if electromagnets are incorporated in the origami structures.

Note that the stability profiles play an important role in determining the mechanical properties (e.g., structural stiffness) and functionalities. Origami structures with controllable stability profiles can therefore be exploited for developing devices and metamaterials with re-programmable properties and multiple functionalities. For example, the proposed approach can be used in aerospace structures [40] to obtain improved morphing capabilities and adaptive stiffness characteristics. The controllable stability profile is also beneficial in the dynamic regime. Rather than offering a single dynamic functionality, multiple functions can be achieved in the same structure by simply controlling the underlying stability profile via magnets. For example, the magnet-coupled origami structure can be bistable and utilized as an energy harvester, since the characteristic snap-through oscillations in a bistable system is beneficial for effective and broadband harvesting; on the other hand, the same structure can be controlled to be mono-stable so that it can serve as a vibration isolator.

#### **ACKNOWLEDGMENTS**

This research was supported by the National Science Foundation under Award 1634545 and the University of Michigan Mechanical Engineering Collegiate Professorship.

### **REFERENCES**

- [1] Kuribayashi, K., Tsuchiya, K., You, Z., Tomus, D., Umemoto, M., Ito, T., and Sasaki, M., 2006, "Self-deployable origami stent grafts as a biomedical application of Ni-rich TiNi shape memory alloy foil," Mater. Sci. Eng. A, **419**(1–2), pp. 131–137.
- [2] Peraza-Hernandez, E. A., Hartl, D. J., Malak Jr, R. J., and Lagoudas, D. C., 2014, "Origami-inspired active structures: a synthesis and review," Smart Mater. Struct., 23(9), p. 094001.
- [3] Randall, C. L., Gultepe, E., and Gracias, D. H., 2012, "Self-folding devices and materials for biomedical applications," Trends Biotechnol., **30**(3), pp. 138–146.
- [4] Felton, S., Tolley, M., Demaine, E., Rus, D., and Wood, R., 2014, "A method for building self-folding machines," Science (80-.)., **345**(6197), pp. 644–646.
- [5] Zhakypov, Z., Falahi, M., Shah, M., and Paik, J., 2015, "The design and control of the multi-modal locomotion origami robot, Tribot," Proceedings of the IEEE

- International Conference on Intelligent Robots and Systems, Hamburg, Germany, pp. 4349–4355.
- [6] Schenk, M., Viquerat, A. D., Seffen, K. a., and Guest, S. D., 2014, "Review of Inflatable Booms for Deployable Space Structures: Packing and Rigidization," J. Spacecr. Rockets, 51(3), pp. 762–778.
- [7] Lebée, A., 2015, "From folds to structures, a review," Int. J. Sp. Struct., **30**(2), pp. 55–74.
- [8] Reis, P. M., López Jiménez, F., and Marthelot, J., 2015, "Transforming architectures inspired by origami," Proc. Natl. Acad. Sci., **112**(40), p. 201516974.
- [9] Silverberg, J. L., Evans, A. A., McLeod, L., Hayward, R. C., Hull, T., Santangelo, C. D., and Cohen, I., 2014, "Using origami design principles to fold reprogrammable mechanical metamaterials," Science (80-.)., 345(6197), pp. 647–650.
- [10] Silverberg, J. L., Na, J., Evans, A. A., Liu, B., Hull, T. C., Santangelo, C. D., Lang, R. J., Hayward, R. C., and Cohen, I., 2015, "Origami structures with a critical transition to bistability arising from hidden degrees of freedom," Nat. Mater., 14(4), pp. 389–393.
- [11] Fang, H., Li, S., Ji, H., and Wang, K. W., 2016, "Uncovering the deformation mechanisms of origami metamaterials by introducing generic degree-4 vertices," Phys. Rev. E, **94**(4), p. 043002.
- [12] Fang, H., Chu, S.-C. A., Xia, Y., and Wang, K. W., 2018, "Programmable Self-Locking Origami Mechanical Metamaterials," Adv. Mater., **30**, p. 1706311.
- [13] Fang, H., Li, S., Ji, H., and Wang, K. W., 2017, "Dynamics of a bistable Miura-origami structure," Phys. Rev. E, **95**(5), p. 052211.
- [14] Fang, H., Wang, K. W., and Li, S., 2017, "Asymmetric energy barrier and mechanical diode effect from folding," Extrem. Mech. Lett., 17, pp. 7–14.
- [15] Waitukaitis, S., Menaut, R., Chen, B. G., and van Hecke, M., 2015, "Origami Multistability: From Single Vertices to Metasheets," Phys. Rev. Lett., **114**(5), p. 055503.
- [16] Cai, J., Deng, X., Ya, Z., Jiang, F., and Tu, Y., 2015, "Bistable behavior of the cylindrical origami structure with Kresling pattern," J. Mech. Des., **137**(6), p. 061406.
- [17] Fang, H., Zhang, Y., and Wang, K. W., 2017, "Origami-Based Earthworm-Like Locomotion Robots," Bioinspir. Biomim., 12, p. 065003.
- [18] Findeisen, C., Hohe, J., Kadic, M., and Gumbsch, P., 2017, "Characteristics of mechanical metamaterials based on buckling elements," J. Mech. Phys. Solids, **102**, pp. 151–164.
- [19] Kidambi, N., Harne, R. L., and Wang, K. W., 2017, "Strain energy capture and storage in asymmetrically multistable modular structures inspired by muscle cross-bridges," Smart Mater. Struct., 26(8).

- [20] Rafsanjani, A., Akbarzadeh, A., and Pasini, D., 2015, "Snapping Mechanical Metamaterials under Tension," Adv. Mater., **27**(39), pp. 5931–5935.
- [21] Bende, N. P., Evans, A. A., Innes-Gold, S., Marin, L. A., Cohen, I., Hayward, R. C., and Santangelo, C. D., 2015, "Geometrically controlled snapping transitions in shells with curved creases," Proc. Natl. Acad. Sci. U. S. A., 112(36), pp. 11175–11180.
- [22] Pandey, A., Moulton, D. E., Vella, D., and Holmes, D. P., 2014, "Dynamics of snapping beams and jumping poppers," Europhys. Lett., **105**, p. 24001.
- [23] Yang, K., Harne, R. L., Wang, K. W., and Huang, H., 2014, "Investigation of a bistable dual-stage vibration isolator under harmonic excitation," Smart Mater. Struct., 23(4), p. 045033.
- [24] Harne, R. L., and Wang, K. W., 2017, Harnessing bistable structural dynamics for vibration control, energy harvesting, and sensing, John Wiley and Sons.
- [25] Wu, Z., Harne, R. L., and Wang, K. W., 2014, "Energy harvester synthesis via coupled linear-bistable system with multistable dynamics," J. Appl. Mech., **81**(6), p. 061005.
- [26] Wu, Z., Zheng, Y., and Wang, K. W., 2018, "Metastable modular metastructures for on-demand reconfiguration of band structures and non-reciprocal wave propagation," Phys. Rev. E, **97**, p. 022209.
- [27] Camescasse, B., Fernandes, a., and Pouget, J., 2014, "Bistable buckled beam and force actuation: Experimental validations," Int. J. Solids Struct., **51**(9), pp. 1750–1757.
- [28] Fang, H., and Wang, K. W., 2017, "Piezoelectric vibration-driven locomotion systems Exploiting resonance and bistable dynamics," J. Sound Vib., **391**, pp. 153–169.
- [29] Harne, R. L., and Wang, K. W., 2014, "A bifurcation-based coupled linear-bistable system for microscale mass sensing," J. Sound Vib., 333(8), pp. 2241–2252.
- [30] Li, S., and Wang, K. W., 2015, "Fluidic origami with embedded pressure dependent multi-stability: a plant inspired innovation," J. R. Soc. Interface, **12**(111), p. 20150639.
- [31] Yasuda, H., and Yang, J., 2015, "Reentrant origamibased metamaterials with negative Poisson's ratio and bistability," Phys. Rev. Lett., **114**(18), pp. 1–5.
- [32] You, Z., and Cole, N., 2006, "Self-locking bi-stable deployable booms," 47th AIAA/ASME/ASCE/AHS/ASC Struct. Struct. Dyn. Mater. Conf. 14th AIAA/ASME/AHS Adapt. Struct. Conf. 7th, (May), pp. 1–10.
- [33] Li, S., and Wang, K. W., 2015, "Fluidic origami: a plant-inspired adaptive structure with shape morphing and stiffness tuning," Smart Mater. Struct., **24**(10), p. 105031.

- [34] Crivaro, A., Sheridan, R., Frecker, M., Simpson, T. W., and Lockette, P. Von, 2014, "Bistable Compliant Mechanism Using Magneto Active Elastomer Actuation," Proc. ASME 2014 Int. Des. Eng. Tech. Conf. Comput. Inf. Eng. Conf. (IDETC/CIE 2014), pp. 1–9.
- [35] Zhao, J., Zhang, Y., Huang, Y., Liu, S., Chen, G., Gao, R., and Yang, Y., 2014, "Mechanical-Magnetic Coupling Analysis of a Novel Large Stroke Penta-Stable Mechanism Possessing Multistability Transforming Capability," J. Mech. Robot., 6(3), p. 031004.
- [36] Bowen, L., Springsteen, K., Feldstein, H., Frecker, M., Simpson, T. W., and von Lockette, P., 2015,
   "Development and Validation of a Dynamic Model of Magneto-Active Elastomer Actuation of the Origami Waterbomb Base," J. Mech. Robot., 7(1), p. 011010.
- [37] Sung, E., Erol, A., Frecker, M., and Lockette, P. Von, 2016, "Characterization of Self-Folding Origami Structures Using Magneto-Active Elastomers,"

- Proceedings of the ASME 2016 International Design Engineering Technical Conferences and Computers and Information in Engineering Conference, pp. 2016–59919.
- [38] Cowan, B. M., 2015, "Magnetically induced actuation and optimization of the Miura-ori structure," The Pennsylvania State University.
- [39] Ahmen, S., Lauff, C., Crivaro, A., McGough, K., Sheridan, R., Frecker, M., Lockette, P. von, Ounaies, Z., Simpson, T., Lien, J.-M., and Strzelec, R., 2013, "Multi-field respinsive origami structures: preliminary modeling and experiments," Proceedings of the ASME 2013 International Design Engineering Technical Conferences and Computers and Information in Engineering Conference, pp. DETC2013-12405.
- [40] Kuder, I. K., Arrieta, A. F., Raither, W. E., and Ermanni, P., 2013, "Variable stiffness material and structural concepts for morphing applications," Prog. Aerosp. Sci., 63, pp. 33–55.

10